GPR wave field decomposition, synthesis and imaging for lossless layered vertically transverse isotropic media

Evert Slob and Kees Wapenaar
Department of Geoscience & Engineering
Delft University of Technology, Delft, The Netherlands
Email: e.c.slob@tudelft.nl; c.p.a.wapenaar@tudelft.nl

***Abstract*—In this paper a scheme is presented to process 3D ground-penetrating radar reflection data acquired on a surface above a vertical transverse isotropic layered medium. The processing steps first decompose the data into Transverse Electric and Transverse Magnetic modes and up and down going waves, where the two modes are fully separated and can be treated separately in the two following steps. The first step that follows is wave field synthesis, where a virtual receiver is constructed in the layered subsurface at any depth level, from which is virtual vertical radar profile can be constructed. This can be done down to the depth level where the waves generated from the upper half space can reach as propagating waves. Once the up and down going vertical radar profiles are obtained at this virtual receiver position, well-known interferometry by deconvolution is used as a second step to obtain an image containing local primary reflection coefficients as a function of incidence angle of the initial plane wave. A numerical example demonstrates the effectiveness of removing multiples from the data and constructing an image free of effects of such internal multiple reflections.**

I. Introduction

Ground penetrating radar is increasingly being used to provide quantitative information of layered structures. For application in civil engineering these can be roads, highway pavements, airport runways, bridges, tunnels, or buildings. Monitoring is important for the management and safety of these structures. For high-resolution imaging and inversion methods wave field processing of reflection data is necessary. This requires acquisition geometries with multiple source and receiver positions laid out in a grid on a surface.

A wave field processing method known as data-driven focusing in 1D is based on inverse scattering theory [1], [2]. Based on the results of Marchenko type inversion of reflection data in 1D [3], [4] has recently resulted in schemes for creating virtual vertical seismic profiles with a virtual receiver at depth where no physical source or receiver has been placed [5], [6], [7]. These schemes can be used as a basis to derive 3D Marchenko type schemes for eliminating internal multiples in seismic migration [8], [9].

Here the derivation is modified and applied to the situation of a layered medium where the layers can be characterized by different horizontal and vertical electric permittivity and magnetic permeability values inside each layer. The necessary processing steps are described and analyzed. It is shown how measurements of all four horizontal components of the electromagnetic field measured with a multi-input multi-ouput acquisition system can be decomposed into up and down going waves where the TE- and TM-modes are separated from each other and treated independently after the first step. The wavefield is focused inside the layered medium by creating a virtual receiver at a certain depth level and it is shown how this leads to the construction of a virtual vertical radar profile with the virtual receiver at a chosen depth level and the source at the location of the original source. The down going and up going wave fields at the virtual receiver level are obtained separately and can be used in an imaging scheme that creates a subsurface image by deconvolving the up gong VRP Green's function by the down going VRP green's function in a similar way as previously derived [10], [11]. This approach is similar to but distinctly different from [12] who described a direct inverse method on plane wave electromagnetic data that cannot be implemented numerically for data with finite bandwidth. A numerical example illustrates the theory presented here and investigates the resolution capabilities of thin layers and the effects of finite bandwidth data.

II. Wave field decomposition

In a vertical transverse isotropic (VTI) layered medium the TE- and TM-modes are independent modes that can be separated. The wave fields can be solved for separately after which the electric and magnetic fields can be found by combining the two solutions. This is briefly shown here in the horizontal wavenumber frequency domain. First we give the expression of Maxwell's equations in this domain [13]

$$\eta^{(v)}\tilde{E}_z = -\tilde{J}^e_z - \hat{\boldsymbol{z}}\cdot(\mathrm{i}\boldsymbol{k}_T\times\tilde{\boldsymbol{H}}_T), \tag{1}$$

$$\zeta^{(v)}\tilde{H}_z = -\tilde{J}^m_z + \hat{\boldsymbol{z}}\cdot(\mathrm{i}\boldsymbol{k}_T\times\tilde{\boldsymbol{E}}_T), \tag{2}$$

$$\eta\tilde{\boldsymbol{E}}_T = -\tilde{\boldsymbol{J}}^e_T + \hat{\boldsymbol{z}}\times\partial_z\tilde{\boldsymbol{H}}_T - \mathrm{i}\boldsymbol{k}_T\times\hat{\boldsymbol{z}}\tilde{H}_z, \tag{3}$$

$$\zeta\tilde{\boldsymbol{H}}_T = -\tilde{\boldsymbol{J}}^m_T - \hat{\boldsymbol{z}}\times\partial_z\tilde{\boldsymbol{E}}_T + \mathrm{i}\boldsymbol{k}_T\times\hat{\boldsymbol{z}}\tilde{E}_z. \tag{4}$$

where $\tilde{E}_z, \tilde{H}_z$ and $\tilde{J}^e_z, \tilde{J}^m_z$ denote the vertical components of the electric and magnetic fields and sources, $\tilde{\boldsymbol{E}}_T, \tilde{\boldsymbol{H}}_T$ and $\tilde{\boldsymbol{J}}^e_T, \tilde{\boldsymbol{J}}^m_T$ the electric and magnetic field and source vectors with subscript $_T$

meaning that the vectors contain only the horizontal components, e.g. $\tilde{\boldsymbol{E}}_T = (\tilde{E}_x, \tilde{E}_y, 0)$, and $\boldsymbol{k}_T$ denotes the horizontal wave number vector. The electric and magnetic medium parameters in the horizontal and vertical directions are given by $\eta = \sigma + \mathrm{i}\omega\varepsilon, \zeta = \mathrm{i}\omega\mu$, $\eta^{(v)} = \sigma^{(v)} + \mathrm{i}\omega\varepsilon^{(v)}, \zeta^{(v)} = \mathrm{i}\omega\mu^{(v)}$, respectively. The vertical derivative is denoted ∂_z and $\hat{\boldsymbol{z}}$ denotes the unit vector in the vertical direction and points downward. Equation (1) represents the TM-mode while equation (2) represents the TE-mode. These two modes can be separated by considering scalar TE-mode, $\tilde{\mathcal{E}}_1, \tilde{\mathcal{H}}_1$, and TM-mode, $\tilde{\mathcal{E}}_2, \tilde{\mathcal{H}}_2$, fields given by

$$\tilde{\mathcal{E}}_1 = -\hat{\boldsymbol{z}} \cdot \left(\frac{\mathrm{i}\boldsymbol{k}_T}{\kappa} \times \tilde{\boldsymbol{E}}_T \right), \qquad \tilde{\mathcal{H}}_1 = \frac{\mathrm{i}\boldsymbol{k}_T}{\kappa} \cdot \tilde{\boldsymbol{H}}_T, \tag{5}$$

$$\tilde{\mathcal{E}}_2 = \frac{\mathrm{i}\boldsymbol{k}_T}{\kappa} \cdot \tilde{\boldsymbol{E}}_T, \qquad \tilde{\mathcal{H}}_2 = \hat{\boldsymbol{z}} \cdot \left(\frac{\mathrm{i}\boldsymbol{k}_T}{\kappa} \times \tilde{\boldsymbol{H}}_T \right), \tag{6}$$

where $\kappa = \sqrt{k_x^2 + k_y^2}$ denote the radial wavenumber. From these equations the vertical electric and magnetic fields can be recovered directly from equations (1) and (2), whereas the horizontal electric and magnetic field components are retrieved by weighted combinations of equations (5) and (6). The sources are now given by

$$\tilde{\boldsymbol{\mathcal{X}}}_1 = \begin{pmatrix} \tilde{\mathcal{X}}_{11} \\ \tilde{\mathcal{X}}_{12} \end{pmatrix} = \begin{pmatrix} -\frac{\mathrm{i}\boldsymbol{k}_T}{\kappa} \cdot \hat{\boldsymbol{I}}_T^m \\ \hat{\boldsymbol{z}} \times \frac{\mathrm{i}\boldsymbol{k}_T}{\kappa} \cdot \hat{\boldsymbol{I}}_T^e - (\zeta^v)^{-1} \kappa \hat{I}_z^m, \end{pmatrix}, \tag{7}$$

$$\tilde{\boldsymbol{\mathcal{X}}}_2 = \begin{pmatrix} \tilde{\mathcal{X}}_{21} \\ \tilde{\mathcal{X}}_{22} \end{pmatrix} = \begin{pmatrix} -\frac{\mathrm{i}\boldsymbol{k}_T}{\kappa} \cdot \hat{\boldsymbol{I}}_T^e \\ -\hat{\boldsymbol{z}} \times \frac{\mathrm{i}\boldsymbol{k}_T}{\kappa} \hat{\boldsymbol{I}}_T^m - (\eta^v)^{-1} \kappa \hat{I}_z^e, \end{pmatrix}, \tag{8}$$

where we have assumed the sources are point sources given by $\tilde{\boldsymbol{J}}^{e,m}(\boldsymbol{k}_T, z, z^s, \omega) = \hat{\boldsymbol{I}}^{e,m}(\omega)\delta(z - z^s)$. Now the can write the TE-and TM-mode field equations as a matrix vector equation given by

$$\partial_z \tilde{\boldsymbol{F}}_{1,2} + \tilde{\mathbf{A}}_{1,2} \tilde{\boldsymbol{F}}_{1,2} = \tilde{\boldsymbol{\mathcal{X}}}_{1,2} \delta(z - z^s). \tag{9}$$

The TE-mode field equations are obtained when we take $\tilde{\boldsymbol{F}}_1 = (\tilde{\mathcal{E}}_1, \tilde{\mathcal{H}}_1)^t$, where ^{t} denotes matrix transposition, and the TM-mode equations are obtained with $\tilde{\boldsymbol{F}}_2 = (\tilde{\mathcal{H}}_2, \tilde{\mathcal{E}}_2)^t$, while the source vectors are defined in equations (7) and (8) and the system matrices are given by

$$\tilde{\mathbf{A}}_1 = \begin{pmatrix} 0 & \zeta \\ \Gamma_1^2/\zeta & 0 \end{pmatrix}, \qquad \tilde{\mathbf{A}}_2 = \begin{pmatrix} 0 & \eta \\ \Gamma_2^2/\eta & 0 \end{pmatrix}, \tag{10}$$

where the vertical wave numbers are given by $\Gamma_1^2 = \zeta(\kappa^2 + \zeta^{(v)}\eta)/\zeta^{(v)}$, and $\Gamma_2^2 = \eta(\kappa^2 + \zeta\eta^{(v)})/\eta^{(v)}$. It is noted that the TE-mode does not depend on $\zeta^{(v)}$ while the TM-mode does not depend on $\eta^{(v)}$. Solving the TE-mode problem directly solves the TM-mode problem based on electromagnetic equivalence [14]. Finally it is noted that the wave equation for either TE-mode or TM-mode only depends on the radial wave number.

Here the solution for the TE-mode is given without using the subscript $_1$ in the remainder of this abstract. The first step toward the solution is to diagonalize the wave equation using an eigenvalue decomposition such that $\tilde{\mathbf{A}} = \mathbf{L}\mathbf{\Lambda}\mathbf{L}^{-1}$, where $\tilde{\mathbf{\Lambda}}$ is the diagonal eigenvalue matrix, and the field vector $\tilde{\boldsymbol{F}}$ is composed from up going and down going wave field components as $\tilde{\boldsymbol{F}} = \tilde{\mathbf{L}}\tilde{\boldsymbol{P}}$ and $\tilde{\boldsymbol{P}} = \tilde{\mathbf{L}}^{-1}\tilde{\boldsymbol{F}}$. We use flux normalization such that

$$\tilde{\mathbf{L}} = \begin{pmatrix} \sqrt{\zeta/\Gamma} & \sqrt{\zeta/\Gamma} \\ \sqrt{\Gamma/\zeta} & -\sqrt{\Gamma/\zeta} \end{pmatrix} \quad \tilde{\mathbf{L}}^{-1} = \frac{1}{2} \begin{pmatrix} \sqrt{\Gamma/\zeta} & \sqrt{\zeta/\Gamma} \\ \sqrt{\Gamma/\zeta} & -\sqrt{\zeta/\Gamma} \end{pmatrix}. \tag{11}$$

$\tilde{\mathbf{\Lambda}} = \mathrm{diag}(\Gamma, -\Gamma)$. Using these decompositions in the TE-mode wave equation of equation (9) gives $\partial_3 \tilde{\boldsymbol{P}} + \tilde{\mathbf{\Lambda}}\tilde{\boldsymbol{P}} = \tilde{\boldsymbol{X}}\delta(x_3 - x_3^S)$, with $\tilde{\boldsymbol{X}} = \tilde{\mathbf{L}}^{-1}\tilde{\boldsymbol{\mathcal{X}}}$ the decomposed source vector. The vectors can be written as $\tilde{\boldsymbol{P}} = (\tilde{P}^+, \tilde{P}^-)^t$ and $\tilde{\boldsymbol{X}} = (\tilde{X}^+, \tilde{X}^-)^t$, where the superscripts $^+,^-$ denote a down going, and up going component, respectively. The continuity conditions apply to the TE-mode field components across any source free boundary in the layered model. The discrete layered earth solution in the upper half space, $z < 0$, for this system is well-known and can be written as

$$\tilde{P}_0^+(z) = \begin{cases} 0 \\ \tilde{X}^+ \exp(-\Gamma_0 h^-) \end{cases}, \tag{12}$$

$$\tilde{P}_0^-(z) = \begin{cases} \tilde{X}^- \exp(-\Gamma_0 h^-) + R_0 \tilde{X}^+ \exp(\Gamma_0 h^+) \\ R_0 \tilde{X}^+ \exp(\Gamma_0 h^+) \end{cases}, \tag{13}$$

where the subscript $_0$ denotes the layer index, defined as layer $\mathbb{D}_i$ is described by depth values $z_{i-1} < z < z_i$. The vertical distances are given by $h^- = |z - z^s|$ and $h^+ = z + z^s$ for $z < 0$ and R_0 denotes the reflection response of the layered medium at the top interface at depth level $z = 0$. The first row is valid for $z < z^s$ and the second for $z^S < z < 0$ for $\tilde{P}_0^{\pm}$. In the remainder it is assumed that the GPR data is recorded in such a way that this decomposition is possible. In case the receiver are at or below the source level it is possible to retrieve the subsurface reflection response R_0 from the measured data as $R_0 = \tilde{P}_0^-/\tilde{P}_0^+$ assuming $h^{\pm}$ and the propagation velocity in the upper half space are known from the acquisition configuration [15]. Note that this decomposition is possible even when the finite size of transmitting and receiving antennas are taken into account, because antenna size would merely amount to limiting the available spatial bandwidth.

III. Wave field synthesis

From now on the layered medium is assumed lossless, hence $\sigma = 0$ everywhere in the layered model. For a point in the subsurface, at depth level $z_i > 0$ the up going wave field at the receiver level z_i of the corresponding vertical radar profile (VRP) can be obtained from the reflection response in the following form [16]

$$\tilde{G}^-(\alpha, z_i, 0, \omega) = [\tilde{R}(\alpha, 0, 0, \omega) - \tilde{R}_i(\alpha, 0, 0, \omega)]\tilde{T}^{-1}(\alpha, 0, z_i, \omega), \tag{14}$$

where $\tilde{G}^-(\alpha, z_i, 0, \omega)$ denotes the upgoing wavefield measured at depth level z_i generated by a plane wave source emitting a wave at incidence angle α at $z = 0$ as a function of reflection and

transmission responses. The notation is slightly changed relative to the previous section, $\tilde{R}(\alpha,0,0,\omega) = R_0$ as defined in equation (13) represents the reflection response of the layered medium for a down going point source at depth level $z = 0$ and the up going field is measured at the same depth level. The function $\tilde{R}_i(\alpha,0,0,\omega)$ denotes the reflection response with down going source and receiver at level $z = 0$ of the medium that is the same layered medium as the real medium from the upper half space down to level $z = z_i$, but is homogeneous below that level, $z > z_i$ and $\tilde{T}(\alpha,0,z_i,\omega)$ denotes to total transmission response in this reduced medium. The homogeneous lower half space of the reduced medium has the same properties as the actual medium just below z_i.

Because flux-normalization is used $\tilde{T}(\alpha,0,z_i,\omega) = \tilde{T}(\alpha,z_i,0,\omega)$, meaning it is irrelevant whether the source is at $z = z_i$ and the receiver at $z = 0$ or the other way around. The angle, α, is defined as the angle of incidence of the plane wave in the upper half space and corresponds to the wave number frequency value under investigation, $\kappa = \omega\sin(\alpha)/c_0$ where $c_0 = 1/\sqrt{\varepsilon_0\mu_0^v}$ denotes the wave propagation velocity in the horizontal direction in the upper half space. For a layer $\mathbb{D}_i$ the vertical wave number can be written as $\Gamma_i = \mathrm{i}\omega\tilde{q}_i(\alpha)$ in which the vertical slowness is given by $\tilde{q}_i(\alpha) = \sqrt{\zeta_i(1/c_i^2 - \sin(\alpha)]^2/c_0^2)/\zeta_1^{(v)}}$, and the propagation velocity the horizontal direction in layer $\mathbb{D}_i$ is given by $c_i = \sqrt{\varepsilon_i\mu_i^{(v)}}$. From equation (14) it can be seen that knowledge of $\tilde{R}_i(\alpha,0,0,\omega)/\tilde{T}(\alpha,0,z_i,\omega)$ and $1/\tilde{T}(\alpha,0,z_i,\omega)$ would be sufficient to construct the up going wave field of the virtual VRP from the measured total reflection response of a layered medium.

The transmission response of a layered medium across the whole medium always consists of a single direct arrival followed by a coda that contains all possible multiple reflections inside the layered medium. The coda can be represented as a denominator in a fractional description of the transmission response [16]. This implies that the inverse of the transmission response contains a finite number of terms, each representing an event in space-time. The reflection response on one side of this same layered medium can be written in fractional form with the same finite number of terms in the numerator and denominator. The denominator of the reflection response is the same as the denominator of the transmission response and the ratio of the reflection and transmission responses also has a finite number of terms. Both the inverse transmission response and the ratio of reflection and transmission responses have the same number of finite terms leading to a finite amount of events in space-time and the first non-zero event occurs at $t = -t_d(\alpha,0,z_i)$ where t_d denotes the one-way vertical intercept time, which is an apparent arrival time. For real values of q_{i+1} the wave propagates across the reduced layered medium and the inverse transmission response consists of propagating events. In that case $t_d(\alpha,0,z_i) = \sum_{n=1}^{i}\tilde{q}_i(\alpha)(z_n - z_{n-1})$ and is half the two-way vertical intercept time of the recorded primary reflection event in the measured data. Two-way intercept time is the recording time when the data is transformed to the horizontal-slowness time domain. For precritical angles of incidence $\tilde{q}_i(\alpha)$ is a real and positive parameter and leads to a real and positive time value. We will therefore restrict further analysis to precritical angles of incidence.

For waves that propagate across the first i layers of the layered medium a second relation can be found that expresses the down going wave field in the subsurface as if the down going wave field is measured at $z = z_i$ and generated by a down going point source at $z = 0$ and the reflection and transmission responses between the levels $z = 0$ and $z = z_i$. This is achieved by using the reciprocity theorem of the time-correlation type for one-way wave fields, which for the up going and down going wave fields in a layered medium is given by [17]

$$[\tilde{P}_A^+(\alpha,0,\omega)]^*\tilde{P}_B^+(\alpha,0,\omega) - [\tilde{P}_A^-(\alpha,0,\omega)]^*\tilde{P}_B^-(\alpha,0,\omega) =$$

$$[\tilde{P}_A^+(\alpha,z_i,\omega)]^*\tilde{P}_B^+(\alpha,z_i,\omega) - [\tilde{P}_A^-(\alpha,z_i,\omega]^*\tilde{P}_B^-(\alpha,z_i,\omega), \quad (15)$$

where * denotes complex conjugation. For state A the reduced medium is taken that is the same as the real medium from the upper half space down to z_i and homogeneous below it. We then have $\tilde{P}_A^+(\alpha,0,\omega) = \tilde{T}^{-1}(\alpha,0,z_i,\omega)$, $\tilde{P}_A^-(\alpha,0,\omega) = \tilde{R}_i(\alpha,0,0,\omega)\tilde{T}^{-1}(0,z_i,\omega)$, and $\tilde{P}_A^+(\alpha,z_i,\omega) = 1$, while $\tilde{P}_A^-(\alpha,z_i,\omega) = 0$. In state B we take the actual configuration and use $\tilde{P}_B^+(\alpha,0,\omega) = 1$, $\tilde{P}_B^-(\alpha,0,\omega) = \tilde{R}(\alpha,0,0,\omega)$ and $\tilde{P}_B^\pm(\alpha,z_i,\omega) = \tilde{G}^\pm(\alpha,z_i,z_0,\omega)$. The desired equation is obtained if we substitute these choices in equation (15). We find

$$\hat{G}^+(\alpha,z_i,0,\omega) = \Big(1 - \tilde{R}(\alpha,0,0,\omega)[\tilde{R}_i(\alpha,0,0,\omega)]^*\Big) \times [T^{-1}(\alpha,0,z_i,\omega)]^*. \quad (16)$$

Equation (16) constructs the downgoing wavefield at receiver level z_i, that is generated by a unit amplitude down going plane wave at the top, from the measured reflection response $\tilde{R}(\alpha,0,0,\omega)$ and the functions $\tilde{T}^{-1}(\alpha,0,z_i,\omega)$ and $\tilde{R}_i(\alpha,0,0,\omega)/\tilde{T}(\alpha,0,z_i,\omega)$. Summing equations (14) and (16) yields the VRP data for a receiver at z_i and a source at $z = 0$ in the actual layered medium.

Transforming equations (14) and (16) to the time domain leads to two coupled equations. First the functions $\tilde{f}^\pm(\alpha,0,z_i,\omega)$ are introduced as $\tilde{f}^+(\alpha,0,z_i,\omega) = \tilde{T}^{-1}(\alpha,0,z_i,\omega)$, being the down going wave field from the upper half space incident on the reduced layered medium, and $\tilde{f}^-(\alpha,0,z_i,\omega) = \tilde{R}_i(\alpha,0,0,\omega)/\tilde{T}^{-1}(\alpha,0,z_i,\omega)$ is the up going wave field just above the top interface and is the reflection response of the reduced layered model in response to $\tilde{f}^+$. The time-domain equivalents of

equations (14) and (16) are given by

$$G^-(\alpha, z_i, 0, t) = -f^-(\alpha, 0, z_i, t) + \int_{t'=-t_d(\alpha,0,z_i)}^{t} f^+(\alpha, 0, z_i, t')R(\alpha, 0, 0, t-t')\mathrm{d}t', \quad (17)$$

$$G^+(\alpha, z_i, 0, t) = f^+(\alpha, 0, z_i, -t) - \int_{t'=-t_d(\alpha,0,z_i)}^{t} f^-(\alpha, 0, z_i, -t')R(\alpha, 0, 0, t-t')\mathrm{d}t'. \quad (18)$$

The integration interval is finite because the two functions in the integrands are non-zero only in a subinterval. The global reflection response $R(0, 0, t-t')$ is causal and therefore zero-valued for $t' > t$, putting the upper limit at $t' = t$. The functions $f^{\pm}$ are non-zero only in the interval $-t_d(\alpha, 0, z_i) \leq t \leq t_d(\alpha, 0, z_i)$. In fact, the incident wave field has its first arrival at $t = -t_d(\alpha, 0, z_i)$ followed by a coda and can be expressed as

$$f^+(\alpha, 0, z_i, t) = \mathcal{T}_d^{-1}(\alpha, 0, z_i)\delta(t + t_d(\alpha, 0, z_i)) + f_1^+(\alpha, 0, z_i, t), \quad (19)$$

where $\mathcal{T}_d(\alpha, 0, z_i) = \prod_{n=0}^{i} \tau_n(\alpha)$ in which $\tau_n(\alpha)$ is the local transmission coefficient across interface n in either direction. It is understood that $f_1^+(\alpha, 0, z_i, t) = 0$ for $|t'| \geq t_d(\alpha, 0, z_i)$. Because the reflection response is the response to f^+ it will also be zero in the interval where f_1^+ is zero, hence $f^-(\alpha, 0, z_i, t) = 0$ for $|t'| \geq t_d(\alpha, 0, z_i)$. The Green's functions $G^{\pm}$ are zero before the first arrival, which arrives at $t = t_d(\alpha, 0, z_i)$. This implies that the functions f_1^+ and f^- can be found on their interval $-t_d(\alpha, 0, z_i) < t < t_d(\alpha, 0, z_i)$. In this way the measured reflection response of the actual medium is used to find the desired functions in the reduced medium using equations (17) and (18). Once these are found the same equations can then be used on the interval $t \geq t_d(\alpha, 0, z_i)$ to determine the Green's functions. Hence first we evaluate

$$f^-(0, z_i, t, \alpha) = \mathcal{T}_d^{-1}(0, z_i)R(0, 0, t + t_d(\alpha, 0, z_i)) + \int_{t'=-t_d(\alpha,0,z_i)}^{t} f_1^+(0, i, t', \alpha)R(0, 0, t-t', \alpha)\mathrm{d}t', \quad (20)$$

$$f_1^+(0, z_i, -t, \alpha) = \int_{t'=-t_d(\alpha,0,z_i)}^{t} f^-(0, z_i, -t', \alpha)R(0, 0, t-t', \alpha)\mathrm{d}t', \quad (21)$$

valid for $-t_d(\alpha, 0, z_i) < t < t_d(\alpha, 0, z_i)$. The Green's functions can then be found for $t \geq t_d(\alpha, 0, z_i)$ from equations (17) and (18).

IV. Wave field imaging

For imaging the two Green's functions can be used, because they represent the wave fields that correspond to up and down going waves at subsurface depth level z_i that are generated by a source in the upper half space. Previous studies on interferometry by multidimensional deconvolution techniques have shown that [15]

$$G^-(\alpha, z_i, 0, t) = \int_{t'=t_d(\alpha,0,z_i)}^{t} R(\alpha, z_i, z_i, t-t')G^+(\alpha, z_i, 0, t')\mathrm{d}t', \quad (22)$$

for $t \geq t_d(\alpha, 0, z_i)$ and $R(\alpha, z_i, z_i, t)$ denotes the reflection response of the layered medium that is the same as the actual medium below z_i while it is homogeneous above z_i and where the integration bounds are determined by causality of the reflection response and the Green's function. The image $\mathcal{I}(\alpha, z_i)$ with the amplitude of the local reflection coefficient just below depth level z_i is obtained by deconvolving equation (22) for the reflection response and evaluating the result at $t = 0$, hence

$$\mathcal{I}(\alpha, z_i) = R(\alpha, z_i, z_i, t = 0). \quad (23)$$

Hence, the image is obtained with only the local primary reflection coefficient at the correct depth and no effects of multiple reflections are present in the final image result. Notice that to find the image at the correct depth the one-way arrival time of the direct event $t_d(\alpha, 0, z_i)$ must be known and this can be done by performing velocity analysis on the 3D data from which very good estimates of depth level z_i can be obtained for a given time t_d. Depending on the frequency bandwidth and the available angles of incidence a high-resolution image can be obtained with correct local amplitudes as a function of incidence. On these results amplitude-versus-angle amplitude analysis can be performed to find the the electric permittivity and magnetic permeability values inside every layer. In this situation the image can also first be obtained as a function of apparent vertical travel time, $t_d(\alpha, 0, z_i)$ which is half the recording time hence the image times are known exactly. Once the image is obtained and the electric permittivity and magnetic permeability values are obtained inside all layers the image times can be converted to depth values. This latter would constitute an inversion step, but is beyond the scope of this paper.

From the equations it is clear that the theory assumes infinite bandwidth, which cannot be achieved with real data. It is therefore important to investigate the effects of finite bandwidth on the results. This is treated in the next section

V. Numerical implementation and results

The reflection response that can be retrieved by processing measured data will have a limited frequency bandwidth depending on the antennas used. Let the frequency bandwidth be determined by the filter function $\hat{W}(\omega, \omega_c)$ where ω_c denotes the radial center frequency. For pulsed radar the filter is a smooth function of frequency and can often be approximated by a Ricker wavelet given by

$$\hat{W}(\omega, \omega_c) = 4\sqrt{\pi}\frac{\exp(-(\omega/\omega_c)^2)}{\omega_c(\omega/\omega_c)^2}, \quad (24)$$

ε_0, μ_0
$\varepsilon_1 = 3.9\varepsilon_0, \mu_1 = \mu_0, d_1 = 1.57m$
$\varepsilon_2 = 2.4\varepsilon_0, \mu_2 = \mu_0, d_2 = 0.21m$
$\varepsilon_3 = 4.2\varepsilon_0, \mu_3 = \mu_0, d_3 = 1.7m$
$\varepsilon_4 = 9.1\varepsilon_0, \mu_4 = 1.4\mu_0, d_4 = 1.21m$
$\varepsilon_5 = 16.1\varepsilon_0, \mu_5 = 1.75\mu_0, d_5 = 1.1m$
$\varepsilon_6 = 12.3\varepsilon_0, \mu_6 = 1.93\mu_0, d_6 = 1.23m$
$\varepsilon_7 = 9.1\varepsilon_0, \mu_7 = 1.5\mu_0, d_7 = 1.51m$
$\varepsilon_8 = 13.3\varepsilon_0, \mu_8 = 2.31\mu_0$

Fig. 1. Layered model with parameter values for permittivity, magnetic permeability, and layer thickness.

such that the wavelet peak amplitude in the time domain is unity. For the example a 125 MHz center frequency is used. The layered model is an isotropic medium with eight interfaces and seven homogeneous layers of finite thickness, of which the second layer is thin relative to the dominant wavelength with the parameters given in Figure 1. The velocity structure is the highest velocity is in the upper half space where the source is located, which is the usual situation for surface ground penetrating radar measurements. This also implies that propagating waves in the upper half space can always propagate throughout the layered medium. The acquisition geometry is assumed to be large enough to allow a maximum angle of incidence of 35^o in the upper half space, which leads to a propagation angle of just over 4^o in the three layers with the lowest propagation velocity and the maximum propagation angle of 15^o occurs in the thin fast layer. At the center frequency the thin layer is less than one seventh of the wavelength. The horizontal components of the electric and magnetic fields are recorded and decomposed in up and down going TE- and TM mode wave fields from which the TE-mode is used to determine the TE-mode reflection response by deconvolving the up going field by the down going field. In this way the presence of the antenna source time signature is removed, but of course only within the available bandwidth, and the bandwidth is smoothed using the 125 MHz Ricker wavelet specified in equation (24). The resulting reflection response is given by

$$\bar{R}(\alpha, 0, 0, t) = \int_{t'=0} R(\alpha, 0, 0, t')\hat{W}(t - t', \omega_c)\mathrm{d}t'. \quad (25)$$

Using this definition equations (20) and (21) can be rewritten for the band limited reflection response and can be solved by discretization and matrix inversion, but an iterative scheme will be more advantageous. The initial estimate can be obtained as

$$\bar{f}_0^-(0, z_i, t, \alpha) = \mathcal{T}_d^{-1}(0, z_i)\bar{R}(0, 0, t + t_d(\alpha, 0, z_i)), \quad (26)$$

$$\bar{f}_{1;0}(0, z_i, t, \alpha) = 0. \quad (27)$$

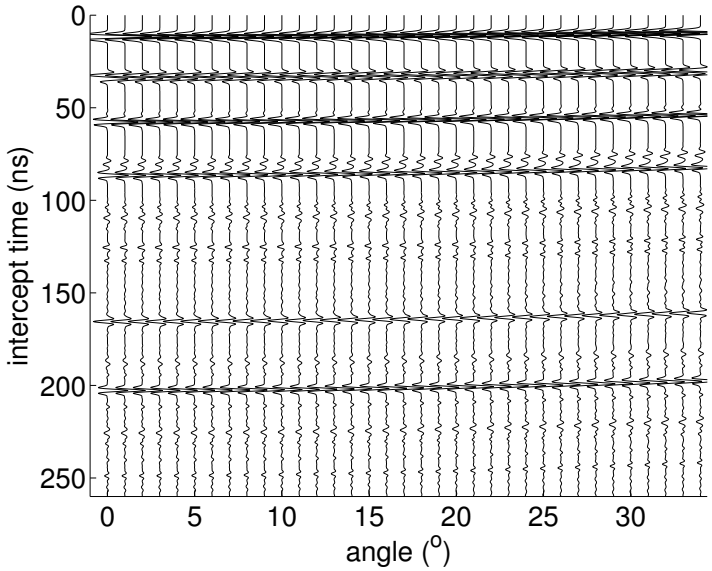

Fig. 2. The reflection response as a function of incidence angle and two-way intercept time.

Then the n^{th} iteration can be evaluated for $n \geq 1$ as

$$\bar{f}_n^-(0, z_i, t, \alpha) = \bar{f}_0^-(0, z_i, t, \alpha) + \int_{t'=-t_d(\alpha,0,z_i)}^{t} \bar{f}_{1;n-1}^+(0, i, t', \alpha)R(0, 0, t - t', \alpha)\mathrm{d}t', \quad (28)$$

$$\bar{f}_{1;n-1}^+(0, z_i, -t, \alpha) = \int_{t'=-t_d(\alpha,0,z_i)}^{t} \bar{f}_n^-(0, z_i, -t', \alpha)R(0, 0, t - t', \alpha)\mathrm{d}t'. \quad (29)$$

Notice that now both R and $\bar{R}$ occur and that R should be understood as the numerically deconvolved version of $\bar{R}$, because R is only known within the available bandwidth. The bandwidth information is present in $\bar{f}$, which is defined in the same way as $\bar{R}$ is defined in equation (25). These functions can be discretized in a straightforward manner and the time-convolution integrals are evaluated using an FFT-algorithm.

The band limited TE-mode reflection response is input data as a function of incidence angle and two-way intercept time as shown in Figure 2. The data consists of primary and multiple reflections and especially in the time window between 100 ns and 150 ns primary and multiple reflections cannot be distinguished. The functions $f^{\pm}$ are computed by iteratively solving equations (28) and (29) and for the model given in Figure 1 the number of coupled iterations is nine for all image times that are computed in the time window from 0 ns to 200 ns and this number is constant for all angles of incidence considered. In Figure 3 the result is shown after the deconvolution step and applying the imaging condition of equations (22) and (23)

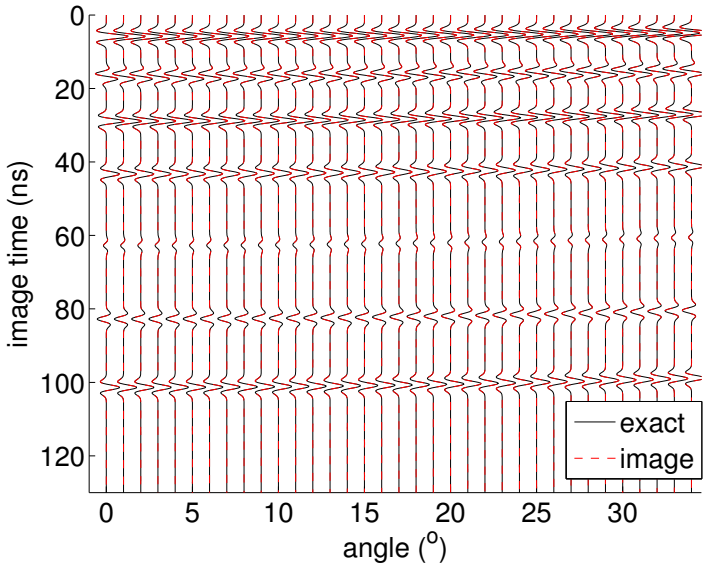

Fig. 3. The image as a function of incidence angle and one-way intercept time, black solid lines indicate the exact result and the red dotted lines indicate the numerical result.

up to an image time of 130 ns, to demonstrate that the scheme remains stable after the latest primary event has arrived and only multiples are left in the data. rom the figure it can be seen that the small amplitude primary reflection that has an image time just larger than 60 ns is well retrieved while all multiple events have disappeared from the image. Thirdly, the convoluted two primaries corresponding to the top and bottom of the thin layer and which have an image time just before 20 ns has been accurately imaged as well. How well multiples can be removed from real measured data will depend on the signal-to-noise ratio.

VI. Conclusion

A method has been presented for processing multi-offset 3D GPR reflection data measured on a surface above a layered medium that does not dissipate electromagnetic wave energy. The first step decomposes the data in TE- and TM-mode up and down going waves and each mode wave field can be processed separately after this this step. The following step consists of determining functions that can be used to synthesize virtual vertical radar profiles as if the receiver was placed at a chosen depth in the subsurface while the source remains at its original position. The virtual VRP is obtained for up and down going waves separately at the subsurface receiver level. From these two functions known multidimensional deconvolution can be used to form an image that is free from subsurface multiple reflection effects. Numerical results demonstrate that for data with finite bandwidth the scheme can be adapted to work accurately, that thin layers can be resolved within the available bandwidth while still removing internal multiple effects, and the small amplitude reflection events are accurately imaged. We further argued that from the image amplitudes, amplitude-versus-angle analysis may lead to accurate local inversions. Only filter steps are involved and the information is obtained from the data.

Acknowledgment

This research has been performed in the framework of the Active and Passive Microwaves for Security and Subsurface imaging (AMISS) EU 7th Framework Marie Curie Actions IRSES project (PIRSES-GA-2010-269157). This abstract is part of the research program of the Netherlands research center for Integrated Solid Earth Science.

References

[1] J. H. Rose, "Single-sided autofocusing of sound in layered materials," *Inverse Problems*, vol. 18, pp. 1923–1934, Dec 2002.

[2] F. Broggini, R. Snieder, and K. Wapenaar, "Focusing the wavefield inside an unknown 1D medium: Beyond seismic interferometry," *Geophysics*, vol. 77, no. 5, pp. A25–A28, September-October 2012.

[3] Z. S. Agranovich and V. A. Marchenko, *The inverse problem of scattering theory*. New York: Gordon and Breach, 1963.

[4] G. L. Lamb, *Elements of Soliton Theory*. New York: John Wiley & Sons Inc., 1980.

[5] F. Broggini, R. Snieder, and K. Wapenaar, "Connection of scattering principles: focusing the wavefield without source or receiver," in *SEG Technical Program Expanded Abstracts*, 2011, pp. 3845–3850.

[6] F. Broggini and R. Snieder, "Connection of scattering principles: a visual and mathematical tour," *European Journal of Physics*, vol. 33, no. 3, pp. 593–613, MAY 2012.

[7] K. Wapenaar, F. Broggini, and R. Snieder, "Creating a virtual source inside a medium from reflection data: heuristic derivation and stationary-phase analysis," *Geophysical Journal International*, vol. 190, no. 2, pp. 1020–1024, AUG 2012.

[8] K. Wapenaar, J. Thorbecke, J. van der Neut, E. Slob, F. Broggini, and R. Snieder, "Integrated migration and internal multiple elimination," in *SEG Technical Program Expanded Abstracts*, 2012, p. SPMUL1.5.

[9] K. Wapenaar, F. Broggini, E. Slob, and R. Snieder, "Three-dimensional single-sided marchenko inverse scattering, data-driven focusing, green's function retrieval, and their mutual relations," *Physical Review Letters*, vol. 110, p. 084301, Feb 2013. [Online]. Available: http://link.aps.org/doi/10.1103/PhysRevLett.110.084301

[10] E. Holvik and L. Amundsen, "Elimination of the overburden response from multicomponent source and receiver seismic data, with source designature and decomposition in PP-, PS-, SP- and SS-wave responses," *Geophysics*, vol. 70, pp. SI11–SI21, 2005.

[11] K. Wapenaar, E. Slob, and R. Snieder, "Seismic and electromagnetic controlled-source interferometry in dissipative media," *Geoph. Prosp.*, vol. 56, no. 3, pp. 419–434, 2008.

[12] S. Coen, "Inverse scattering of permittivity and permeability profiles of a plane stratified medium," *Journal of Mathematical Physics*, vol. 22, no. 5, pp. 1127–1129, 1981.

[13] J. Kong, "Electromagnetic fields due to dipole antennas over stratified anisotropic media," *Geophysics*, vol. 37, no. 6, pp. 985–996, 1972.

[14] J. A. Kong, *Electromagnetic Wave Theory*. New York: John Wiley & Sons, 1986.

[15] E. Slob, "Interferometry by deconvolution of multi-component multi-offset GPR data," *IEEE Trans. Geoscience and Remote Sensing*, vol. 47, no. 3, pp. 828–838, March 2009.

[16] P. L. Goupillaud, "An approach to inverse filtering of near surface effects from seismic records," *Geophysics*, vol. 26, no. 6, pp. 754–760, 1961.

[17] C. P. A. Wapenaar and J. L. T. Grimbergen, "Reciprocity theorems for one-way wavefields," *Geophysical Journal International*, vol. 127, no. 1, pp. 169–177, OCT 1996.